A. Methods details

As GRAPPA is frequently used in current MR scanners, it is necessary to include it in the comparison. We perform grid search of GRAPPA parameters that yield the highest possible SSIM and PSNR, namely kernel size 7×7 and the parameter for the kernel calibration $\gamma = 0.01$. For the U-Net, the pre-trained weights provided by [23] are used. The weights are trained on the single-coil fastMRI knee data. The same weights are applied to out-of-distribution experiments, as described below. For GRAPPA and the fastMRI U-Net, which reconstruct the image slice by slice, we generate a 3D image by stacking the slices to a 3D volume.

We evaluate the consistency of each method for several under-sampling operators according to specific distributions, namely Uniformly random distribution with acceleration factor $2\times$ and 15% center fraction and Gaussian random distribution with acceleration factor $8\times$ and 8% center fraction, respectively [13, 52]. In order to evaluate the out-of-distribution reconstruction, we use the model that was trained on fastMRI data without any fine-tuning. The model weights provided by DiffusionMBIR [8] are taken for a fair comparison. For fastMRI knee data.

B. Hyper-parameters selection

We perform a grid search to find a good configuration for the hyper-parameters of the Fourier slice optimization, m, η and α. Figure 5 shows the grid search results, where the optimal configuration is found as iteration $m = 10$, regularization parameters for sparsity $\alpha = 0.02$, learning rate $\eta = 0.01$, and including total variation. We this configuration in all empirical evaluations, unless differently specified.

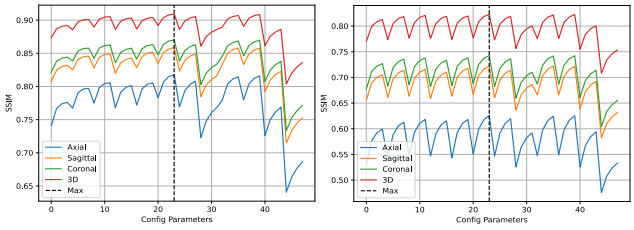

Figure 5. Hyperparameters search for uniform mask (left) and Gaussian mask (right), where the maximum is given in the configuration at index = 23 with combination parameters: ($m = 10, \alpha = 0.02, \eta = 0.01$,tv=1)

C. Ablation Gaussian

Our results are consistent with the Uniform case, where regularization is required to improve the SSIM. This confirms that both regularization terms are contributing to improve the given optimization pipeline.

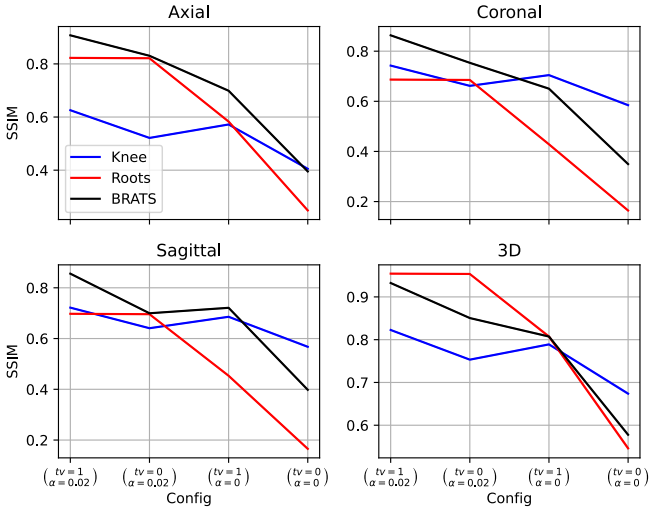

Figure 6. Ablation study to investigate the effect of regularization for reconstruction in terms of SSIM (↑) metric for Gaussian mask. The optimization iteration $m = 10$ and $\eta = 0.01$.

D. 3D MR images and their projection

We follow the definition and presentation of the Fourier slice method as given in [6, 7]. Suppose we have 2D function $p(x, y)$, the projection can be written as

$$p(x) = \int_{-\infty}^{\infty} p(x, y)dy$$

Now observe the 2D Fourier transform $\widehat{p}(k_x, k_y) = \mathcal{F}_{2D}\left(p(x, y)\right)$

$$\widehat{p}(k_x, k_y)) = \int_{-\infty}^{\infty}\int_{-\infty}^{\infty} p(x, y)e^{-2\pi(xk_x+yk_y)}dxdy$$

Focusing on the slice at the center frequency at $y-$axis, i.e., $k_y = 0$, we have

$$\begin{aligned}\widehat{p}(k_x, 0) &= \int_{-\infty}^{\infty}\int_{-\infty}^{\infty} p(x, y)dy\, e^{-2\pi x k_x}dx \\ &= \int_{-\infty}^{\infty} p(x)e^{-2\pi x k_x}dx = \mathcal{F}_{1D}\left(p(x)\right)\end{aligned}$$

This is a 1D Fourier transform on the projection. Additionally, the projection in the discrete setting is the summation on the one axis.

E. Optimization problem details

The algorithm 1 performs an alternating update between the DDPM sampling and the Fourier slice optimization in (5). In this section, we will discuss the implementation details to solve the optimization in (5). The sparsity constraint by using ℓ_1-norm is non-smooth. The implementation of

the regularization function in the optimization problem can be represented as the proximal operator [32], namely the soft thresholding operator. Soft thresholding operator can be written as [16, eq. 15.22].

$$\text{prox}_{\alpha}\left(\boldsymbol{X}\right)=\begin{cases}\frac{\boldsymbol{X}}{|\boldsymbol{X}|}\circ\left(|\boldsymbol{X}|-\alpha\right), & \text{if } |\boldsymbol{X}|\geq\alpha\\ 0, & \text{otherwise,}\end{cases} \tag{7}$$

where α is the pre-determined threshold value. It should be noted that the absolute value is applied element-wise for volumetric data. The combination of the proximal operator and the Lagrangian function is called proximal gradient method [5, 32] described as follows

$$\begin{aligned}&\underset{\boldsymbol{X}\in\mathbb{C}^{S\times N\times N}}{\text{minimize}} && \sum_{s=1}^{S}\left\|\hat{\mathbf{Y}}_s-\mathbf{M}\circ\left(\mathcal{F}_{2D}\left(\mathbf{X}_s\right)\right)\right\|_F^2+\mathcal{R}\left(\boldsymbol{X}\right)\\ &\text{subject to} && \begin{aligned}\hat{\mathbf{y}}_s^{k_y}&=\mathbf{m}^{k_y}\circ\mathcal{F}_{1D}\left(\mathcal{P}_y\left(\mathbf{X}_s\right)\right)\\ \hat{\mathbf{y}}_s^{k_x}&=\mathbf{m}^{k_x}\circ\mathcal{F}_{1D}\left(\mathcal{P}_x\left(\mathbf{X}_s\right)\right)\end{aligned} \quad \text{for } s\in[S]\end{aligned} \tag{8}$$

where the regularization $\mathcal{R}\left(\boldsymbol{X}\right)$ can be written as

$$\begin{aligned}&\alpha\underbrace{\sum_{s=1}^{S}\sum_{i=1}^{N}\sum_{j=1}^{N}|x_{s,i,j}|}_{\text{sparsity}}+\underbrace{\sum_{s=1}^{S}\sum_{i=1}^{N}\sum_{j=1}^{N-1}|x_{s,i,j+1}-x_{s,i,j}|^2}_{\text{smoothness}(\mathcal{TV}(\boldsymbol{X}))}\\ &+\underbrace{\sum_{s=1}^{S}\sum_{i=1}^{N-1}\sum_{j=1}^{N}|x_{s,i+1,j}-x_{s,i,j}|^2}_{\text{smoothness}(\mathcal{TV}(\boldsymbol{X}))}\end{aligned} \tag{9}$$

To summarize, the entire optimization problem can be formulated in (10) and (11). The proximal projection in (10) deals with the ℓ_1- norm, which encourages the sparsity of the reconstructed image. The first term on the right-hand-side of (11) ensures data fidelity on $xy-$plane, while the second and third terms enhance the continuity on $z-$axis. The last term in (11) incorporates smoothness of MR images.

$$\boldsymbol{X}^{(i)}=\text{prox}_{\alpha}\left(\boldsymbol{X}^{(i-1)}-\lambda\nabla_{\boldsymbol{X}^{(i-1)}}\widehat{L}\left(\boldsymbol{X}^{(i-1)}\right)\right)\in\mathbb{C}^{S\times N\times N} \tag{10}$$

where the function $\widehat{L}\left(\boldsymbol{X}\right)$ can be written as

$$\begin{aligned}\widehat{L}\left(\boldsymbol{X},\rho\right)=&\frac{1}{2}\sum_{s=1}^{S}\left\|\hat{\mathbf{Y}}_s-\mathbf{M}\circ\left(\mathcal{F}_{2D}\left(\mathbf{X}_s\right)\right)\right\|_F^2\\ &+\frac{1}{2}\sum_{s=1}^{S}\left\|\hat{\mathbf{y}}_s^{k_y}-\mathbf{m}^{k_y}\circ\mathcal{F}_{1D}\left(\mathcal{P}_y\left(\mathbf{X}_s\right)\right)\right\|_2^2\\ &+\frac{1}{2}\sum_{s=1}^{S}\left\|\hat{\mathbf{y}}_s^{k_x}-\mathbf{m}^{k_x}\circ\mathcal{F}_{1D}\left(\mathcal{P}_x\left(\mathbf{X}_s\right)\right)\right\|_2^2\\ &+\mathcal{TV}\left(\boldsymbol{X}\right)\end{aligned} \tag{11}$$

In general the function $\mathcal{G}\left(\boldsymbol{X}\right)$ in (5) can be written as in (10). In Appendix B, we will discuss the choosing of hyperparameter, such as learning rate λ, proximal parameters α, and the optimization iteration m, as well as the effect on the regularization function.

F. Qualitative results

In Figure 7 the maximum intensity projections on each axis are displayed to visualize the fine roots structure. In addition, we report the average SSIM and PSNR for each view (axial, coronal, sagittal). It is evident that the fastMRI U-Net struggles to reconstruct the image in areas with limited information, regardless of Uniform or Gaussian masking in the column direction. Besides achieving the highest SSIM and PSNR, the proposed method generates a high-contrast image with minimal pixel-wise differences compared to other methods, as depicted in the bottom-left subplots.

Figure 8 illustrates the reconstruction of BRATS data for each view, accompanied by SSIM and PSNR values for each slice. The figure highlights that DiffusionMBIR yields smaller deviations in error differences with the ground truth, as depicted in the lower left corner box. However, it also introduces higher background noise compared to the proposed method. Notably, in the zoomed area with Gaussian masking, the proposed method effectively generates finer details while adhering closely to the ground truth in comparison to its counterparts.

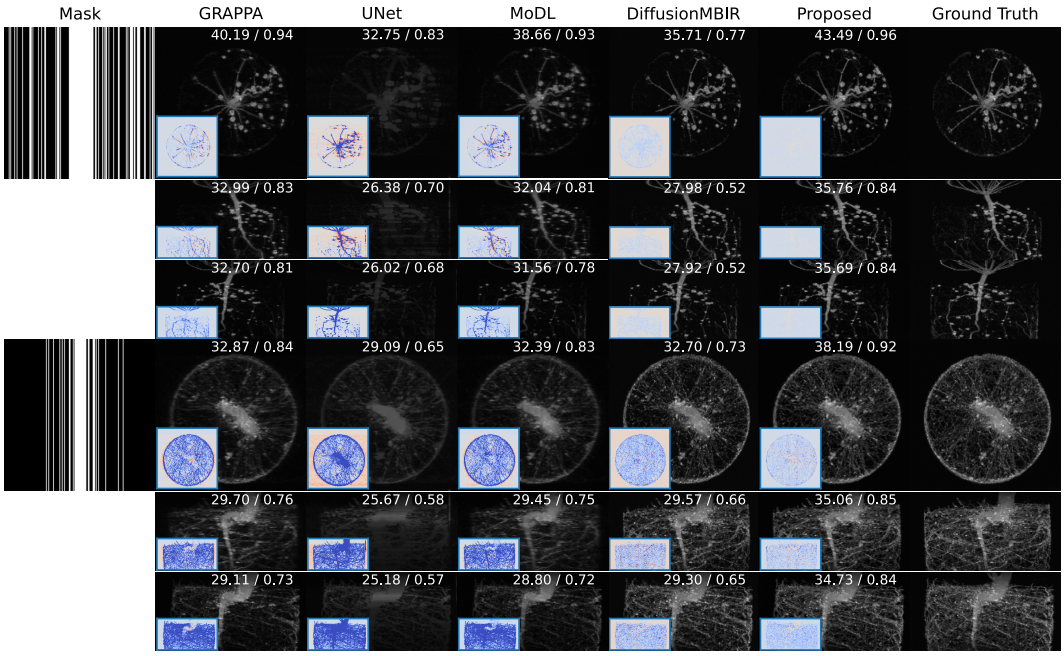

Figure 7. Reconstructions for Lotus (top) and Vicia (bottom) plant roots data. We present vertically the axial, coronal, and sagittal maximum intensity projections. The numbers on the upper right of each image represent the mean PSNR/SSIM of slices along dimensions. The subplots on the lower left are the difference map of the projection w.r.t. the ground truth. The color range is between -0.1 (bluish) and 0.1 (reddish).

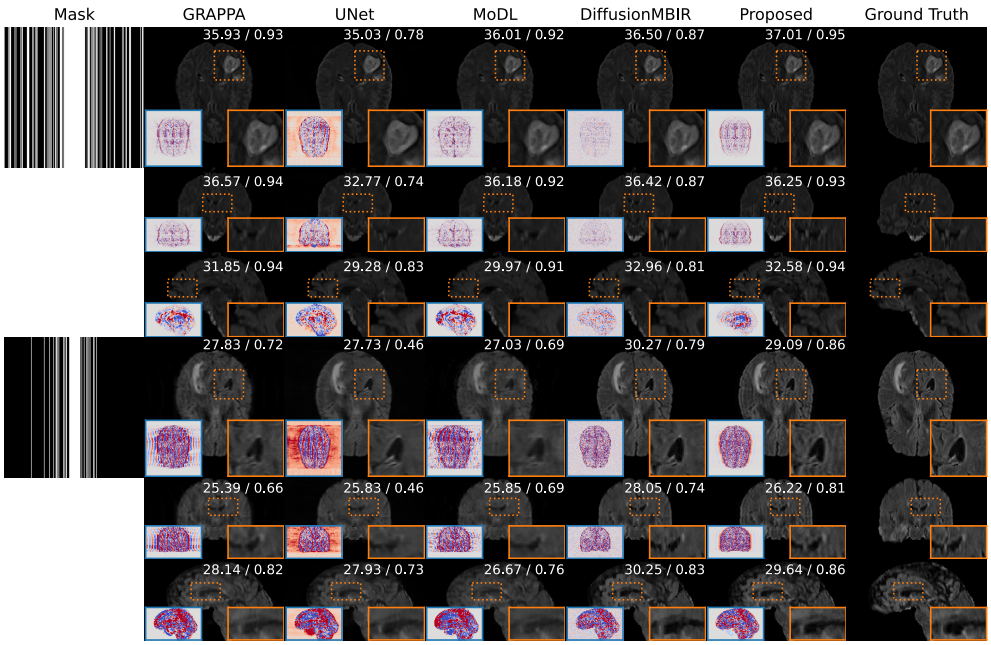

Figure 8. Slices from the volume reconstructions for BRATS data from Brats18_CBICA_APM_1 (top) and Brats18_CBICA_AAM_1 (bottom). We present vertically the axial, sagittal, and coronal middle slices. The numbers on the upper right of each image represent the PSNR/SSIM of middle slices. The subplots on the lower left are the difference map of the projection w.r.t. the ground truth. The color range is between -0.02 (bluish) and 0.02 (reddish).